

Bond disorder and breakdown of ballistic heat transport in the spin-1/2 antiferromagnetic Heisenberg chain as seen in Ca-doped SrCuO₂

N. Hlubek,^{1,*} P. Ribeiro,^{1,*} R. Saint-Martin,² S. Nishimoto,¹ A. Revcolevschi,³ S.-L. Drechsler,¹ G. Behr,^{1,†} J. Trinckauf,¹ J. E. Hamann-Borrero,¹ J. Geck,¹ B. Büchner,¹ and C. Hess^{1,‡}

¹*IFW-Dresden, P.O. Box 270116, D-01171 Dresden, Germany*

²*Laboratoire de Physico-Chimie de L'Etat Solide, ICMMO, UMR8182, Université Paris-Sud, F-91405 Orsay, France*

³*Laboratoire de Physico-Chimie de L'Etat Solide, ICMMO, UMR8182, Université Paris-Sud, 91405 Orsay, France*

(Dated: February 18, 2022)

We study the impact of a weak bond disorder on the spinon heat transport in the $S = 1/2$ antiferromagnetic (AFM) Heisenberg chain material Sr_{1-x}Ca_xCuO₂. We observe a drastic suppression in the magnetic heat conductivity κ_{mag} even at tiny disorder levels (i.e., Ca-doping levels), in stark contrast to previous findings for κ_{mag} of $S = 1/2$ two-dimensional square lattice and two-leg spin-ladder systems, where a similar bond disorder has no effect on κ_{mag} . Hence, our results underpin the exceptional role of integrability of the $S = 1/2$ AFM Heisenberg chain model and suggest that the bond disorder effectively destroys the ballistic nature of its heat transport. We further show that the suppression of κ_{mag} is captured by an effective spinon-impurity scattering length, which exhibits the same doping dependence as the long-distance exponential decay length of the spin-spin correlation as determined by density-matrix renormalization group calculations.

PACS numbers: 75.40.Gb, 66.70.-f, 75.10.Kt, 75.10.Pq

I. INTRODUCTION

The transport properties of the integrable one-dimensional (1D) $S = 1/2$ antiferromagnetic (AFM) XXZ chain model are attracting considerable attention because anomalous spin and heat transports have been predicted.^{1–12} Rigorous predictions concern the *heat* transport of the model in the isotropic (Heisenberg) case. It is known to be *ballistic* as the consequence of integrability and fundamental conservation laws.^{2–5} This means, a *divergent* heat conductivity is expected. However, in experimental realizations of this model, the observable spinon heat conductivity κ_{mag} always has to be finite since extrinsic scattering processes due to defects and phonons are inherent to all materials and mask the intrinsic behavior of a spin chain. Nevertheless, a very large κ_{mag} has been observed in a number of cuprates that realize $S = 1/2$ spin chains.^{13–18} Especially, the material SrCuO₂ is considered an excellent realization of the 1D-AFM $S = 1/2$ Heisenberg model (HM).^{19–21} For this material, we recently reported quasi ballistic spinon heat transport with mean-free paths $l_0 > 1 \mu\text{m}$ for samples of extraordinary purity.¹⁸

Recently, several theoretical studies focused on the consequences of disorder for transport in 1D systems with controversial results.^{22–26} Experimental studies are scarce and, so far, only concern heat transport studies on the 1D-AFM $S = 1/2$ HM with site disorder (diagonal disorder), which cuts the chain into finite segments and, thus, rather trivially leads accordingly to a suppression of transport.¹⁷ Here, we study the more subtle *bond disorder* (off-diagonal disorder), which leaves the chains in the material intact and which recently has been investigated in nuclear magnetic resonance (NMR) experiments.^{27,28} We

induce this subtle type of disorder in SrCuO₂ by systematically substituting isovalent Ca for Sr in tiny amounts. This off-chain lattice doping by small Ca²⁺ ions induces a local lattice distortion which must result in a modulation, i.e., disorder, of the magnetic exchange constant J . In contrast to other doping schemes where the dopants occupy Cu sites within the magnetic structures and, thus, generate site disorder,^{17,29,30} for this bond disorder, one generally expects only subtle changes in the magnetic transport properties of the system. In fact, previous studies show that the magnetic heat transport of the $S = 1/2$ AFM square lattice²⁹ and the two-leg spin ladder systems,³¹ whose underlying spin models are non integrable, is unaffected by such kinds of disorder. Radically different from these findings, in Ca-doped SrCuO₂, we observe a severe suppression of κ_{mag} already at tiny doping levels ($\sim 1\%$). Hence, these data suggest that the disorder-induced departure from integrability efficiently destroys the ballistic nature of heat transport in the 1D-AFM $S = 1/2$ HM. In the framework of a kinetic model, we show that this suppression is captured by an effective spinon-impurity term in the spinon mean-free path, which surprisingly exhibits the same doping dependence as the long-distance decay length of the spin-spin correlation as determined by density-matrix renormalization group (DMRG) calculations.

II. EXPERIMENTAL DETAILS

We have grown centimeter sized single crystals of Sr_{1-x}Ca_xCuO₂ with $x = 0, 0.0125, 0.025, 0.05, 0.1$ using the traveling-solvent floating zone method.³² As starting materials we used CuO (99.99% purity), SrCO₃ (99%

purity) and CaCO_3 (99% purity). Additionally, crystals with $x=0, 0.0125$ were grown with all starting powders of 4N (99.99%) purity. The crystallinity and the doping profile were checked under polarized light and by energy dispersive x-ray spectroscopy. A structural refinement was performed for samples of SrCuO_2 and $\text{Sr}_{0.9}\text{Ca}_{0.1}\text{CuO}_2$ in a single-crystal diffractometer. For the doped material, this yielded a reduction in the cell volume by 1% with respect to the undoped compound in agreement with literature values.³³ Furthermore, we found a change in the Cu-O-Cu bond angle and the bond distance of roughly 0.3%³⁹. Since these data represent averages over the entire crystal volume, we estimated the *local* Ca-induced variation in the lattice from density-functional calculations using the code QUANTUM ESPRESSO.³⁴ A $2 \times 2 \times 2$ supercell of SrCuO_2 doped with 10% Ca was relaxed with minimal symmetry assumptions. This yielded a Cu-O-Cu bond length variation that is approximately the same as the doping induced change in the mean Cu-O-Cu distances measured with the single-crystal diffractometer. This consistency corroborates the presence of a bond disorder in the material. For the transport measurements, rectangular samples with typical dimensions of $(3 \cdot 0.5 \cdot 0.5)$ mm³ for measurements of the heat conductivity along the principal axes (κ_a , κ_b , κ_c) were cut from the crystals for each doping level with an abrasive slurry wire saw. The longest dimension was taken parallel to the measurement axis. Measurements of the thermal conductivity as a function of temperature T in the range of 7–300 K were performed with a standard four probe technique³⁵ using a differential Au/Fe-Chromel thermocouple for determining the temperature gradient.

III. EXPERIMENTAL DATA

Figure 1 shows our experimental results for κ_c and κ_a of $\text{Sr}_{1-x}\text{Ca}_x\text{CuO}_2$ for all doping levels. In the pristine material ($x = 0$), the heat conductivity parallel to the spin chains κ_c is strongly enhanced with respect to the purely phononic heat conductivity perpendicular to the chains κ_a . This is a result from quasi ballistic spinon heat transport in the chains.¹⁸ More specifically, the spinon heat conductivity κ_{mag} , which dominates the total (spinon plus phonon) heat conductivity along the c axis leads to a broad peak at low temperatures ($\kappa_c \approx 830 \text{ Wm}^{-1}\text{K}^{-1}$ at $T \approx 28 \text{ K}$) followed by a strong decrease toward a still significantly enhanced value ($\sim 50 \text{ Wm}^{-1}\text{K}^{-1}$) at room temperature.

Upon doping the material with Ca, the thermal conductivity perpendicular to the spin chains (κ_a) is gradually suppressed. This is the typical expectation of increased scattering by phonons off defects.³⁶ Since the Ca^{2+} impurities possess a smaller ionic radius and mass as compared to Sr^{2+} , they act as defects for the phonons.⁴⁰ A much more dramatic change upon doping is observed in κ_c . Already at the lowest doping level of

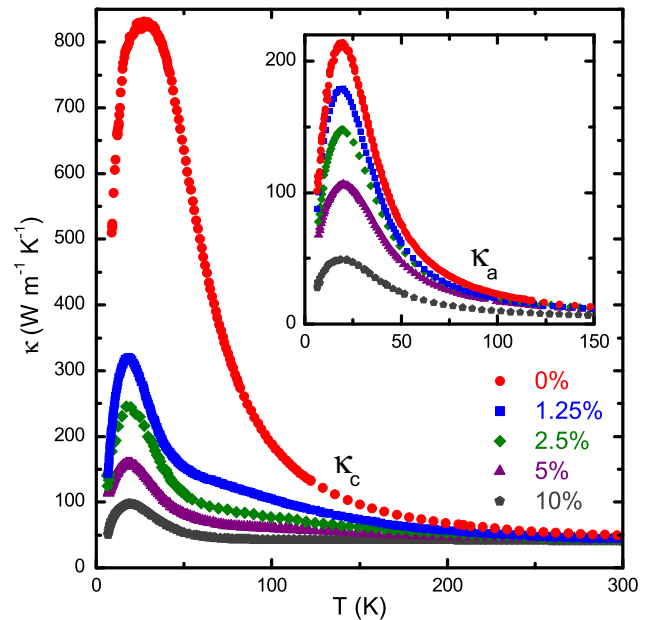


Figure 1: (Color online) Thermal conductivity parallel to the spin chain (κ_c) for $\text{Sr}_{1-x}\text{Ca}_x\text{CuO}_2$ at different doping levels. (Inset) Thermal conductivity for the same doping levels perpendicular to the spin chain (κ_a).

1.25% Ca, κ_c is suppressed strongly as compared to that of the pristine material, and the overall curve shape of $\kappa_c(T)$ is changed completely. The peak at low temperatures is now significantly smaller ($\kappa_c \approx 320 \text{ Wm}^{-1}\text{K}^{-1}$), is much sharper, and is shifted toward lower temperatures ($T \approx 18 \text{ K}$). At about 50 K, κ_c shows a kink, above which, it decreases much weaker and approaches κ_c of the undoped compound for even higher temperatures. Upon increasing the Ca doping, the absolute value of the peak decreases, although its position stays constant. The kink is gradually shifted to higher temperatures, and all of the curves approach the curve of the undoped compound at room temperature. This apparent saturation behavior is most visible at 10% Ca doping, where a small maximum is followed by a practically constant thermal conductivity. Nevertheless, the anisotropy between κ_a and κ_c is still considerable since at 300 K, $\kappa_a \approx 4 \text{ Wm}^{-1}\text{K}^{-1}$ and $\kappa_c \approx 40 \text{ Wm}^{-1}\text{K}^{-1}$.⁴¹

IV. ANALYSIS

The strong suppression of κ_c implies that the Ca impurities lead to a very strong suppression of the spinon heat conductivity κ_{mag} already at very low doping levels ($x \approx 0.01$) because the doping scheme apparently only causes a moderate suppression of the phononic heat conductivity, as seen in κ_a . Qualitatively, this suggests that the doping-induced bond disorder leads to a significant deviation in the spin system in $\text{Sr}_{1-x}\text{Ca}_x\text{CuO}_2$ from the

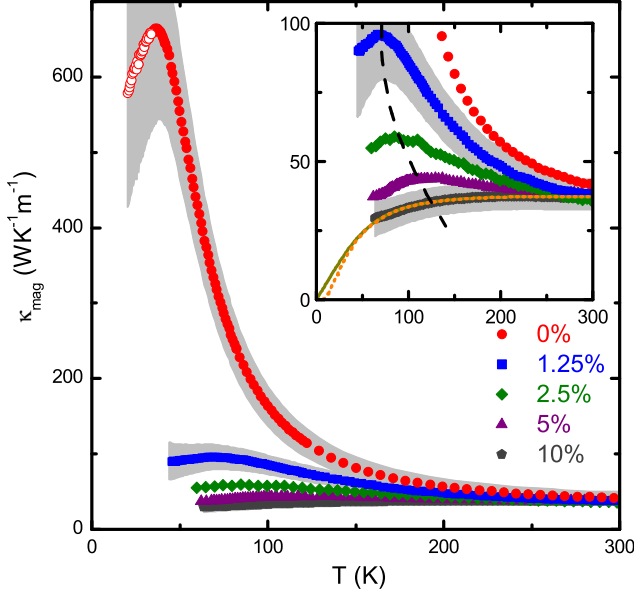


Figure 2: (Color online) κ_{mag} for the different doping levels as a function of temperature. (Inset) Enlarged portion of the main plot shows the different doping levels in more detail. The black dashed line indicates the shift in the maximum to higher temperatures for higher dopings. For 10% Ca doping, an extrapolation is shown without a spin gap (solid yellow line) and with a spin gap of 50 K (dotted orange line). The shaded areas show the uncertainty of the estimation of κ_{mag} due to the phononic background. All curves are shown only down to a temperature for which the uncertainty of the estimation of κ_{mag} is still reasonably small.

$S = 1/2$ Heisenberg chain model, and, thus effectively destroys the ballistic nature of the heat transport in the material. One might conjecture that the connected departure from integrability can be captured by an effective scattering process that describes the observed suppression of κ_{mag} in our heat transport experiments. In order to investigate this notion further, we analyze our data by extracting κ_{mag} and calculating the spinon mean-free path l_{mag} .

A. Spinon heat conductivity

The first step of such an analysis^{13,18} consists in estimating the phononic part of κ_c via $\kappa_{c,\text{ph}} \approx \kappa_a$. Then, the spinon thermal conductivity is given by $\kappa_{\text{mag}} = \kappa_c - \kappa_a$ ⁴². The doping-dependent evolution of κ_{mag} is shown in Fig. 2. At low temperatures, κ_{mag} of the undoped compound shows a large maximum ($\kappa_{\text{mag}} \approx 665 \text{ W m}^{-1} \text{ K}^{-1}$ at $T \approx 36 \text{ K}$), which is followed by a steep decrease upon approaching room temperature where the values of the curve nearly become constant ($\kappa_{\text{mag}} \approx 42 \text{ W m}^{-1} \text{ K}^{-1}$). Doping of 1.25% Ca leads to a severe suppression of κ_{mag} at low temperatures with a broadening of the maximum ($\sim 96 \text{ W m}^{-1} \text{ K}^{-1}$) and a shift to 69 K. Up to room

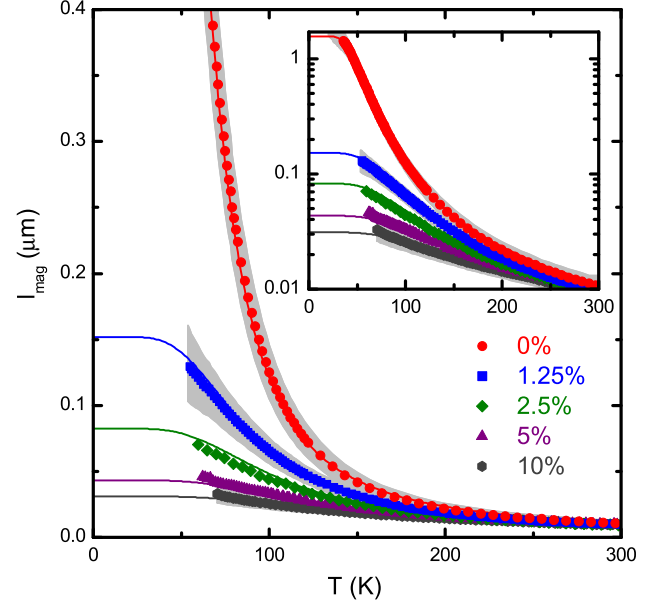


Figure 3: (Color online) l_{mag} of $\text{Sr}_{1-x}\text{Ca}_x\text{CuO}_2$ for different levels of doping. Toward low temperatures, the error in the estimation of κ_{mag} increases due to an increase in κ_{ph} . Thus, the values of l_{mag} are shown only at temperatures above which the error in l_{mag} is reasonably small. The solid lines were calculated according to Eq. (2).

Ca content x	l_0 (Å)	T_u^* (K)	A_s ($10^{-6} \text{ K}^{-1} \text{ m}^{-1}$)	l_0 (c)
0	15596	204	58.7	3989
0.0125	1519	204	65.5	389
0.025	824	204	66.3	211
0.05	433	204	54.8	112
0.1	311	204	50.3	80

Table I: Fit parameters for the mean-free paths according to Eq. (2). Additionally, l_0 is given in units of the lattice constant c .

temperature, the curve approaches that of the undoped compound. Further increasing the doping continues to decrease κ_{mag} at low temperatures and shifts the increasingly broadened maximum to even higher temperatures. For temperatures $T \gtrsim 200 \text{ K}$, the values of κ_{mag} approach those of the undoped compound but remain smaller.

B. Spinon mean free path

For each doping level, we use the derived κ_{mag} data to calculate the spinon mean-free path l_{mag} (see Fig. 3) according to^{13,15,17,18}

$$l_{\text{mag}}(T) = \frac{3\hbar}{\pi N_s k_B^2 T} \kappa_{\text{mag}}, \quad (1)$$

with $N_s = 4/ab$ as the number of spin chains per unit area. For all doping levels, $l_{\text{mag}}(T)$ decreases strongly with increasing temperature which is the signature of

spinon-phonon scattering.^{13,18} However, upon increasing the doping level, l_{mag} exhibits a systematic reduction, and the overall temperature-dependent change at a given doping level becomes less pronounced, suggesting an increased importance of spinon-defect scattering.¹⁸ We test this notion by applying Matthiessen's rule and decomposing l_{mag} into two respective contributions, i.e., $l_{\text{mag}}^{-1}(T) = l_0^{-1} + l_{\text{sp}}(T)^{-1}$. Here, l_0 accounts for temperature-independent spinon-defect scattering, whereas, $l_{\text{sp}}(T)$ corresponds to T -dependent spinon-phonon scattering. By using $l_{\text{sp}}^{-1} \propto T \exp(-T_u^*/T)$ with a characteristic phonon energy scale T_u^* on the order of the Debye temperature,^{13,17,18} we have

$$l_{\text{mag}}^{-1}(T) = l_0^{-1} + A_s T \exp(-T_u^*/T), \quad (2)$$

with a proportionality constant A_s . Equation (2) is used to fit the l_{mag} data in Fig. 3, where T_u^* first was determined for the pure compound and then was used as a constant when fitting the data for finite-doping levels. As can be seen in Fig. 3, the fits describe the data very well (see Table I for the fit parameters)⁴³. A remarkable result is that A_s also is constant nearly for all doping levels with a root-mean-square deviation of around 10% of the arithmetic mean value. Thus, the effect of the bond disorder induced by the Ca doping is described well by only one doping-dependent parameter that describes the spinon-defect scattering l_0 and one temperature-dependent spinon-phonon scattering mechanism, which is independent of doping.

Alternatively, for the afore discussed scattering, one might try to attribute the suppressed κ_{mag} to a disorder-induced depletion of thermally excited quasiparticles. In fact, recent NMR measurements provided evidence for a spin gap $\Delta/k_B \approx 50$ K for 10% Ca doping.²⁸ However, the large J makes the effect of this gap on the transport tiny. To illustrate the negligible influence, the inset in Fig. 2 shows an estimate of the impact of a spin gap¹⁵ on κ_{mag} at 10% Ca doping.

Having established that the suppression of κ_{mag} , induced by the bond disorder, indeed can be described by an effective spinon-defect scattering process, in Fig. 4 we investigate how the corresponding scattering length l_0 develops as a function of doping. As can be inferred from the figure, l_0 decreases systematically with doping, following $l_0 = a_1/x + l_{\text{lim}}$, with the scattering strength a_1 and the offset l_{lim} . Note that, while $l_0 \sim 1/x$ is consistent with previous findings for spin-defect doped chains, two-leg spin ladders and 2D square lattices,^{17,29,30} the finding of a finite offset l_{lim} is rather unexpected. Qualitatively, such a finite offset means that the effect of the bond disorder, in terms of defect like scattering, is strong at very small degrees of disorder but becomes increasingly unimportant at larger degrees of disorder. Hence, the effect of the bond disorder is significantly different from that of strong site defects (diagonal disorder), which cut the chains into finite segments.¹⁷

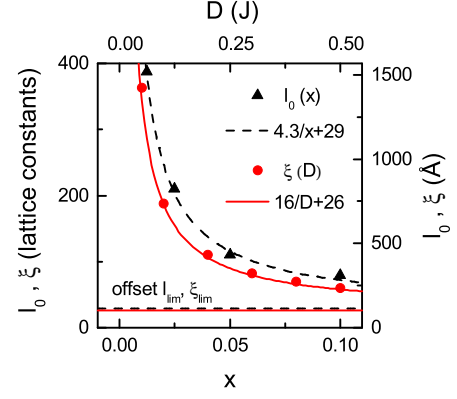


Figure 4: (Color online) l_0 and ξ as a function of doping x (bottom axis) and disorder parameter D (top axis), respectively. The quantities are fitted by $l_0 = a_1/x + l_{\text{lim}}$ ($a_1 \approx 4.3$, $l_{\text{lim}} \approx 29$) and $\xi = a_2/D + \xi_{\text{lim}}$ ($a_2 \approx 16$, $\xi_{\text{lim}} \approx 26$). It is worth noting that only a simple scaling factor for D is necessary to reach an almost perfect agreement between both curves.

C. Spin-spin correlation

In order to obtain deeper insight into the effect of bond disorder on the spin dynamics of the system, we investigated its influence on the spin-spin correlation as a function of the distance z . The model Hamiltonian is written as

$$H = \sum_i (J + D\varepsilon_i) \vec{S}_i \cdot \vec{S}_{i+1}, \quad (3)$$

where \vec{S}_i is a spin- $\frac{1}{2}$ operator at site i , J is the nearest-neighbor exchange interaction without bond disorder, ε_i is defined by a box probability distribution $\mathcal{P}(\varepsilon_i) = \theta(1/2 - |\varepsilon_i|)$ with the step function $\theta(x)$, and the disorder strength is controlled by D . The spin-spin correlation functions $\langle \vec{S}_i \cdot \vec{S}_{i+z} \rangle$ are investigated using the DMRG.³⁷ We study chains with 1024 sites keeping $m = 2000$ density-matrix eigenstates. Here, the open-boundary conditions are used, and the distance z is centered at the middle of the system. We calculate the correlation functions by randomly sampling 300 realizations of $\mathcal{P}(\varepsilon_i) = \theta(1/2 - |\varepsilon_i|)$ and taking an average of the results for each D and z . For $D = 0$, the spin-spin correlation follows a $1/z$ law, which is expected in the ballistic case. For $D > 0$ the long-distance part can be fitted just by $\exp(-z/\xi)$, with the free parameter ξ . Since the commutator of the heat current operator and the spin chain Hamiltonian is no longer zero for $D > 0$, ballistic heat transport no longer is expected. If one interprets the deviation in the spin-spin correlation from the algebraic decay ($1/z$) as a measure for the departure of the system from the clean one (i.e. from integrability), the argument of the fitted exponential may fix the crossover, with $z < \xi$ being ballistic and $z > \xi$ being diffusive. Plotting ξ as a

function of D (cf. Fig. 4) strikingly reveals that ξ depends in the same manner on D as l_0 does on x . Note, in particular, that the calculated offset quantitatively almost perfectly matches that of the experiment, i.e., $\xi \approx l_0$ in the strong disorder or large doping limit. Furthermore, one may apparently assume $D \propto x$. Hence, in the frame of this simple model, the long-distance decay length ξ of the spin-spin correlation can be interpreted as a limit for the effective spinon-defect scattering length l_0 .

V. CONCLUSION

In conclusion, the doping-induced bond disorder in $\text{Sr}_{1-x}\text{Ca}_x\text{CuO}_2$ causes a severe suppression of the spinon heat conductivity which is consistent with a disorder-induced departure of the underlying spin model from integrability and, thus, the destruction of ballistic heat transport. This interpretation is corroborated by the fact that the observed suppression apparently is a characteristic feature of this 1D-AFM $S = 1/2$ HM because no

effect of bond disorder has been observed for a non-integrable $S = 1/2$ AFM square lattice and two-leg ladder systems. Using a simple kinetic model, we have shown that the suppression of κ_{mag} is described well by an effective spinon-defect scattering length, which can be related to the long-distance decay length of the spin-spin correlation as calculated by the DMRG method.

Acknowledgments

We thank W. Brenig, A. L. Chernyshev, and F. Heidrich-Meisner for fruitful discussions. This work was supported by the Deutsche Forschungsgemeinschaft through Grants No. HE3439/7, No. DRE269/3, and No. GE 1647/2-1, through the Forschergruppe FOR912 (Grant No. HE3439/8), and by the European Commission through the projects NOV MAG (Project No. FP6-032980) and the LOTHERM (Project No. PITN-GA-2009-238475).

* These authors contributed equally to this work.

† Deceased.

‡ Electronic address: c.hess@ifw-dresden.de

¹ X. Zotos and P. Prelovšek, Phys. Rev. B **53**, 983 (1996).

² X. Zotos, F. Naef, and P. Prelovšek, Phys. Rev. B **55**, 11029 (1997).

³ X. Zotos, Phys. Rev. Lett. **82**, 1764 (1999).

⁴ A. Klümper and K. Sakai, J. Phys. A **35**, 2173 (2002).

⁵ F. Heidrich-Meisner, A. Honecker, D. C. Cabra, and W. Brenig, Phys. Rev. B **68**, 134436 (2003).

⁶ F. Heidrich-Meisner, A. Honecker, and W. Brenig, Eur. Phys. J. - Spec. Top. **151**, 135 (2007).

⁷ J. Sirker, R. G. Pereira, and I. Affleck, Phys. Rev. Lett. **103**, 216602 (2009).

⁸ S. Grossjohann and W. Brenig, Phys. Rev. B **81**, 012404 (2010).

⁹ M. Žnidarič, Phys. Rev. Lett. **106**, 220601 (2011).

¹⁰ M. Mierzejewski, J. Bonča, and P. Prelovšek, Phys. Rev. Lett. **107**, 126601 (2011).

¹¹ T. Prosen, Phys. Rev. Lett. **106**, 217206 (2011).

¹² J. Sirker, R. G. Pereira, and I. Affleck, Phys. Rev. B **83**, 035115 (2011).

¹³ A. V. Sologubenko, K. Giannò, H. R. Ott, A. Vietkine, and A. Revcolevschi, Phys. Rev. B **64**, 054412 (2001).

¹⁴ P. Ribeiro, C. Hess, P. Reutler, G. Roth, and B. Büchner, J. Mag. Mag. Mater. **290-291**, 334 (2005).

¹⁵ C. Hess, H. ElHaes, A. Waske, B. Büchner, C. Sekar, G. Krabbes, F. Heidrich-Meisner, and W. Brenig, Phys. Rev. Lett. **98**, 027201 (2007).

¹⁶ C. Hess, Eur. Phys. J. Special Topics **151**, 73 (2007).

¹⁷ T. Kawamata, N. Takahashi, T. Adachi, T. Noji, K. Kudo, N. Kobayashi, and Y. Koike, J. Phys. Soc. Jpn. **77**, 034607 (2008).

¹⁸ N. Hlubek, P. Ribeiro, R. Saint-Martin, A. Revcolevschi, G. Roth, G. Behr, B. Büchner, and C. Hess, Phys. Rev. B **81**, 020405(R) (2010).

¹⁹ N. Motoyama, H. Eisaki, and S. Uchida, Phys. Rev. Lett. **76**, 3212 (1996).

²⁰ M. Matsuda, K. Katsumata, K. M. Kojima, M. Larkin, G. M. Luke, J. Merrin, B. Nachumi, Y. J. Uemura, H. Eisaki, N. Motoyama, S. Uchida, and G. Shirane, Phys. Rev. B **55**, R11953 (1997).

²¹ I. A. Zaliznyak, H. Woo, T. G. Perring, C. L. Broholm, C. D. Frost, and H. Takagi, Phys. Rev. Lett. **93**, 087202 (2004).

²² K. Damle, O. Motrunich, and D. A. Huse, Phys. Rev. Lett. **84**, 3434 (2000).

²³ N. Laflorencie, H. Rieger, A. W. Sandvik, and P. Henelius, Phys. Rev. B **70**, 054430 (2004).

²⁴ D. Basko, I. Aleiner, and B. Altshuler, Annals of Physics **321**, 1126 (2006).

²⁵ M. Žnidarič, T. Prosen, and P. Prelovšek, Phys. Rev. B **77**, 064426 (2008).

²⁶ A. Karahalios, A. Metavitsiadis, X. Zotos, A. Gorczyca, and P. Prelovšek, Phys. Rev. B **79**, 024425 (2009).

²⁷ T. Shiroka, F. Casola, V. Glazkov, A. Zheludev, K. Prša, H.-R. Ott, and J. Mesot, Phys. Rev. Lett. **106**, 137202 (2011).

²⁸ F. Hammerath, S. Nishimoto, H.-J. Grafe, A. U. B. Wolter, V. Kataev, P. Ribeiro, C. Hess, S.-L. Drechsler, and B. Büchner, Phys. Rev. Lett. **107**, 017203 (2011).

²⁹ C. Hess, B. Büchner, U. Ammerahl, L. Colonescu, F. Heidrich-Meisner, W. Brenig, and A. Revcolevschi, Phys. Rev. Lett. **90**, 197002 (2003).

³⁰ C. Hess, P. Ribeiro, B. Büchner, H. ElHaes, G. Roth, U. Ammerahl, and A. Revcolevschi, Phys. Rev. B **73**, 104407 (2006).

³¹ C. Hess, C. Baumann, U. Ammerahl, B. Büchner, F. Heidrich-Meisner, W. Brenig, and A. Revcolevschi, Phys. Rev. B **64**, 184305 (2001).

³² A. Revcolevschi, U. Ammerahl, and G. Dhalenne, J. Cryst. Growth **198**, 593 (1999).

- ³³ N. Ohashi, K. Fujiwara, T. Tsurumi, and O. Fukunaga, J. Cryst. Growth **186**, 128 (1998).
- ³⁴ P. Giannozzi, S. Baroni, N. Bonini, M. Calandra, R. Car, C. Cavazzoni, D. Ceresoli, G. L. Chiarotti, M. Cococcioni, I. Dabo, A. Dal Corso, S. de Gironcoli, S. Fabris, G. Fratesi, R. Gebauer, U. Gerstmann, C. Gougousis, A. Kokalj, M. Lazzeri, L. Martin-Samos, N. Marzari, F. Mauri, R. Mazzarello, S. Paolini, A. Pasquarello, L. Paulatto, C. Sbraccia, S. Scandolo, G. Sclauzero, A. P. Seitsonen, A. Smogunov, P. Umari, and R. M. Wentzcovitch, Journal of Physics: Condensed Matter **21**, 395502 (2009).
- ³⁵ C. Hess, B. Büchner, U. Ammerahl, and A. Revcolevschi, Phys. Rev. B **68**, 184517 (2003).
- ³⁶ R. Berman, *Thermal Conduction in Solids* (Clarendon, Oxford, 1976).
- ³⁷ S. R. White, Phys. Rev. Lett. **69**, 2863 (1992).
- ³⁸ C. Hess, C. Baumann, and B. Büchner, J. Mag. Mag. Mater. **290-291**, 322 (2005).
- ³⁹ We find a bond length and angle of 3.910 Å (3.896 Å) and 175.5° (174.9°), respectively, for $x = 0$ ($x = 0.1$).
- ⁴⁰ We also checked the thermal conductivity perpendicular to the chains along κ_b . This gives very similar results apart from a small anisotropy, which is already present in the undoped compound and does not change in magnitude upon doping.
- ⁴¹ Note, that measurements of κ_c with 2N and 4N purity of 1.25% Ca doping did not show any significant difference. Therefore the results for 2.5%, 5% and 10% Ca doping were obtained using crystals of 2N purity.
- ⁴² Considering the small differences between κ_a and κ_b of $\approx 15\%$ compared to the overall anisotropy of more than a factor of 5 between κ_c and κ_a , the validity of this method seems to be justified.
- ⁴³ Modeling the spinon scattering by thermally excited optical phonons^{18,38} achieves a fit of similar quality and comparable l_0 but with different T^* .